HHS Public Access

Author manuscript

Mater Sci Eng C Mater Biol Appl. Author manuscript; available in PMC 2021 August 01.

Published in final edited form as:

Mater Sci Eng C Mater Biol Appl. 2020 August ; 113: 110981. doi:10.1016/j.msec.2020.110981.

Polymeric Nanofibrous Scaffolds Laden with Cell-Derived Extracellular Matrix for Bone Regeneration

Radoslaw Junka[1], **Xiaojun Yu**[1,*]

[1]Department Biomedical Engineering Stevens Institute of Technology, Hoboken, NJ, 07030

Abstract

Bone tissue engineering aims to alleviate the shortage of available autograft material and the biological/mechanical incompatibility of allografts through fabrication of bioactive synthetic bone graft substitutes. However, these substitute grafting materials have insufficient biological potency that limits their clinical efficacy in regenerating large defects. Extracellular matrix, a natural tissue scaffold laden with biochemical and structural cues regulating cell adhesion and tissue morphogenesis, may be a versatile supplement that can extend its biological functionality to synthetic grafts. Embedding decellularized extracellular matrix (dECM) into synthetic polymers offers a promising strategy to enhance cellular response to synthetic materials, mitigate physical and mechanical limitations of dECMs, and improve clinical utility of synthetic bone grafts. Enriched with dECM biochemical cues, synthetic polymers can be readily fabricated into complex biocomposite grafts that mimic bone structure and stimulate endogenous cells to regenerate bone. In this study, cell-derived dECMs from osteoblast and endothelial cells were incorporated into polycaprolactone (PCL) solutions for electrospinning dual-layer nanofibrous scaffolds with osteogenic and vascular cues. The study examined the bioactivity of dECM scaffolds in osteoblast cultures for cell number, mineral deposits, and osteogenic markers, as well as regeneration of cortical bone defect in a rat femur. Scaffolds with osteoblast dECM had a significantly robust osteoblast proliferation, Alizarin Red staining/concentration, and osteopontin-positive extracellular deposits. Implanted scaffolds increased bone growth in femoral defects, and constructs with both osteogenic and vascular cues significantly improved cortical width. These findings demonstrate

(*)**Corresponding Author: Dr. Xiaojun Yu, Ph.D., Associate Professor,** Department of Biomedical Engineering, Stevens Institute of Technology, Hoboken, NJ, 07030, Xiaojun.Yu@stevens.edu, Phone : 201 216 5256, Fax : 201 216 8306.

Author Contributions

R. J. and X.Y. conceptualized and designed the study. R.J. carried out the experimental work. Both authors participated in data analysis, review, and editing of the final manuscript.

Author Statement

Radoslaw Junka: Conceptualization, Methodology, Validation, Formal analysis, Investigation, Data curation, Writing- Original draft preparation, Writing- Reviewing and Editing, Visualization

Xiaojun Yu: Conceptualization , Methodology, Resources, Validation, Formal analysis, Writing- Original draft preparation , Writing- Reviewing and Editing, Funding acquisition, Supervision, Project administration

Conflict of Interests

The authors declare that there is no conflict of interests regarding the publication of this paper.

Declaration of interests

The authors declare that they have no known competing financial interests or personal relationships that could have appeared to influence the work reported in this paper.

the potential to fabricate tailored biomimetic grafts with dECM cues and fibrous architecture for bone applications.

Keywords

Extracellular Matrix; Decellularization; Bone tissue engineering; Osteoblasts; Endothelial Cells; Electrospinning

1. INTRODUCTION

Regeneration of large bone defects poses a major orthopedic challenge. Extensive bone loss and the concurrent damage to surrounding soft tissues disrupt vasculature, alter tissue differentiation, and hinder graft integration with the host tissue. Bone unions fail to form in approximately 10% of long bone fractures and 25–40% of vertebral fusion procedures. [1,2,3] Autologous bone grafting is an effective standard treatment for bone defect reconstruction, but the insufficient availability of a grafting material, donor-site morbidity along with infection risks render this procedure unsuitable in many cases. [4,5] These limitations have prompted the development of bone graft substitutes that mimic bone's native composition and architecture and augment its ability to repair.

The higher success rate of autografts suggest that mimicry of anabolic bone with osteogenic cells grown on an osteoconductive extracellular matrix (ECM) may generate an efficacious bone graft. [6] ECM, a three-dimensional network of protein and polysaccharides embedded in calcium phosphate minerals, constitutes a large portion of bone microenvironment and a substrate for tissue growth. [7] ECM has an inherent multitude of morphological and structural cues that regulate cells adhesion, gene expression, and differentiation. [8,9] Grafts that recapitulate the native bone ECM may be able to guide bone formation with their biochemical signals. Decellularizaton of cell cultures can isolate a broad spectrum of morphological cues that mimic native microenvironment. Decellularized ECM (dECM) retains some of its biochemical complexity, and it exceeds bioactivity of synthetic polymers. [10,11,12,13] Cell-derived dECMs offer flexibility in composition of biological grafts by allowing for combination of dECMs from several cultures to mimic the heterogeneous bone ECM. [14] However, dECMs from homogenous cultures were predominantly evaluated for bone application thus far. [1,15,16,17,18,19]

The mechanical properties of the homogenized dECM hydrogels or powders are insufficient to support regeneration of the hard bone. [20,21] Synthetic bone graft substitutes made from biodegradable and biocompatible materials (ie. polycaprolactone (PCL)) can match the mechanical demands for many orthopedic applications [22]. However, they are void of osteogenic signals which are critical for regeneration of large defects [23]; thus, their effectiveness has proven highly variable. [24] Combining dECM with synthetic biomaterials may remedy the limitations of these materials by tailoring the graft's physical properties using versatile biofabrication techniques and displaying bioactive cues on its surface. [9,25]

Electrospinning is a nanofiber production process used in a variety of applications ranging from textiles, thermal insulators, fuel cells, filtration systems, and tissue engineering

scaffolds [26,27]. This fabrication method has the potential to replicate the fibrous architecture of the bone. [28,29,30]. In bone, type I collagen is arranged in fibrils, a three-dimensional fibrous mesh confirmed in a regular parallel pattern with a diameter distribution between 30 and 80 nm. [31,32] Artificial production of these structures requires processing at a nano-scale and various fiber compositions, including polymer-dECM fibers, were fabricated using the electrospinning. [33,34,35,36,37,38,39] Polymer-dECM fibers can be generated by culturing cells on the electrospun fibers for deposition of ECM on their surface and then decellularizing the culture. [35]. An alternate approach is to embed dECM by lyophilizing the dECM from cell cultures, and blending the powder with a polymer solution for electrospinning.[8,18]

The aim of this study was to combine the manufacturing adaptability of synthetic polymers and the biological diversity of cell-derived dECM to fabricate dual-layer bioactive PCL-dECM nanofibrous scaffolds for bone regeneration. The two-layer scaffolds were fabricated by sequential electrospinning PCL solution containing either osteoblast- or endothelial cells (EC)-derived dECM. Osteoblasts were selected for their capacity to secrete nascent bone ECM components in contrast to undifferentiated MSCs. The evidence of synergistic interactions between EC and osteogenic cells in supporting in tandem bone regeneration and vascularization *in vivo* provided the rationale for incorporation of vascular cues from ECs into scaffolds. Several studies demonstrated that pre-seeding EC together with osteoblasts/bone marrow stem cells can improve mechanical properties of graft, increase capillary density in the graft, and enhance their bone volume fraction and mineralization. [40,41,42,43] Thus, it is likely that ECMs from these two cell types can relay important biological signals that guide bone regeneration. Nanofibers with their high surface to volume ratio are ideal for presentation of a high amount of ECM cues. Prior studies reported a low dECM content with respect to the bulk fiber, ranging from 0.025–1 wt% [8,18,39], while studies with dECM content of 10% or greater used animal sources [8,21,44]. The working hypothesis was that incorporation of both angiogenic and osteogenic cues into nanofibers would produce osteoconductive scaffolds with improved mechanical strength that will stimulate bone growth via ECM-mediated signaling. The hypothesis was tested by characterizing scaffolds' physical and biological properties, and evaluating their capacity to enhance osteoblast proliferation, alkaline phosphatase (ALP) activity, amount of calcium mineral deposits, and osteocalcin (OC) and osteopontin (OPN) markers. *In vivo* bioactivity was evaluated 6 weeks after implantation in a cortical defect of a rat femur by means of histology and histomorphometry. This work demonstrates the potential of tissue mimicry approach using polymer-dECM nanofibrous scaffolds with dECM tunable composition and the physical malleability of synthetic polymers which could be useful in a variety of tissue engineering applications.

2. MATERIALS AND METHODS

2.1. Electrospinning PCL and PCL-ECM nanofibers

For PCL fibers, polycaprolactone (PCL, Mw = 80,000, Sigma) pellets were dissolved in 1,1,1,3,3,3-hexafluoro-2-propanol (HFIP, Oakwood Products) at a 16% (w/v) ratio. For PCL-dECM fibers, PCL fibers decorated with cell-derived dECM were removed from 50

coverslips, dehydrated with ethanol gradient (70%−100%), and dried in a desiccator overnight. The mass of the PCL fibers was measured before and after culture. Dry PCL-dECM fibers were dissolved in HFIP/Formic acid/DMSO (8:1:1 v/v) to obtain solutions that were 16% PCL (w/v) and 10% dECM (w/w). For PCL-collagen fibers, rat tail collagen (C7661, Sigma) was dissolved in HFIP to obtain a 10% collagen (w/w) and 16% (w/v) PCL solution. The solutions were loaded into a 5mL syringe with a 20G blunt stainless steel needle and delivered at a flow rate of 0.25 mL/h using a medical syringe pump. To induce fiber formation, high voltage source was set to 10–12 kV. Fibers were collected on 18 mm glass coverslips placed on an aluminum foil wrapped collector kept at a distance of 10 cm from the needle tip. Electrospinning parameters are summarized in Table 1.

Nanofibrous scaffolds were composed of two connected fiber layers (EC dECM and/or osteo dECM fibers) through sequential electrospinning of above solutions. Five groups of scaffolds were fabricated in the following configurations: (1) osteo dECM fibers (top layer) and EC dECM fibers (bottom layer) (EO), (2) PCL fibers (top layer) and EC dECM fibers (bottom layer) (ENDO), (3) osteo dECM fibers (top layer) and PCL fibers (bottom layer) (OST), (4) PCL fibers (top and bottom layers) (PCL), and (5) PCL/collagen fibers (top layer) and PCL fibers (bottom layer) (COL). A schematic representation of the scaffold fabrication procedure is presented in Figure 1.

2.2. Preparation and decellularization of cell-derived ECM from Osteoblasts and ECs.

Primary rat osteoblasts (Cell Applications, San Diego, CA) were subcultured in α-Minimal Essential Medium supplemented with penicillin (50 U/ml), streptomycin (50 μg/ml) (Gibco), and 10% fetal bovine serum (ATCC) and maintained at 37°C in a humidified atmosphere of 5% CO_2 and 95% air. Primary rat endothelial cells (ECs, Cell Applications, San Diego, CA) were cultured in a supplemented endothelial cell medium without phenol red according to manufacturer's instructions. Prior to seeding, PCL scaffolds were disinfected for 2h in 70% ethanol and washed three times in phosphate buffered saline (PBS, ThermoFisher). Osteoblasts and ECs were seeded onto PCL scaffolds at a density of 10^5 cells/scaffold and cultured for 28 days to allow for secretion of ECM. Culture media was changed every other day. Fibrous constructs from cell cultures with deposited ECM were decellularized according to a previously published protocol after 28 days. [45] Briefly, cultured fibers were washed with PBS three times and placed in a 5 mM phosphate-buffered 68.5 mM sodium solution (½ PBS) containing 125 mM3-(Decyldimethylammonio)-propane-sulfonate (SB-10) overnight at 4°C under gentle agitation. Afterwards, constructs were washed three times in PBS and placed in ½ PBS solution containing 0.14% sodium deoxycholate and 0.6mM 3-(N,N-Dimethylpalmitylammonio) propanesulfonate (SB-16) overnight at 4 °C under gentle agitation. This process was repeated two times. Decellularized constructs were stored in PBS at 4°C.

2.3. Assessment of the DNA and protein content of decellularized ECM scaffolds

Decellularized PCL fibers decorated with dECM were stained with 0.05 % Methylene Blue solution (MB, Sigma) for 20 minutes for DNA detection. [46] Coomassie Blue R250 (CB, Bio-Rad) staining for 1h was used for protein detection. [47] Afterwards, the samples were washed in PBS until nonspecific binding was eliminated. The images were captured using a

Nikon T100 Stereomicroscope. The DNA and protein content was quantified using Quant-iT™ PicoGreen dsDNA (ThermoFisher) [48] and Bicinchoninic acid (BCA) (ThermoFisher) assays [48,49], respectively. Assays were performed according to manufacturer's instructions with some modifications. Fibers with decellularized dECM were detached from coverslips, placed in a 15 mL tube containing 4 mL of working solution for each assay, and vortexed for 1 minute. For BCA, samples were incubated at 37°C for 30 minutes, and the absorbance was measured at 562 nm wavelength. For Quant-iT™, samples were incubated at room temperature for 5 minutes, and fluorescence was measured at 485/530 nm (ex./em.). PCL scaffolds without dECM were used as controls. Standard curves were generated for each test and used to determine DNA and protein amounts. Five samples were tested for each condition.

2.4. Scanning Electron Microscopy (SEM)

Characterization of electrospun fibers was performed using Auriga FE-SEM (Zeiss, Germany). Samples were sputter-coated with gold and imaged at several magnifications using an accelerating voltage of 5 kV. Average fiber diameter and fiber diameter distribution were determined by measuring at least 100 individual fibers from at least 5 different images using ImageJ software (ImageJ 1.49, National Institutes of Health, USA). Average pore size and pore size distribution were determined by thresholding and Analyze Particles module in ImageJ. To examine morphological changes of osteoblasts and ECs after attachment to fibers, scaffolds were removed from culture media 24h after seeding, washed three times with PBS, and fixed with 4% paraformaldehyde solution for 30 mins. Scaffolds were dehydrated in ethanol gradient, dried in a desiccator overnight, sputter-coated with gold, and examined under the SEM operated at 3kV.

2.5. Porosity

For porosity (θ) measurements, scaffolds were cut into ten 2cm^2 samples and measured by the liquid intrusion method. [50] After recording dry weight of samples, they were immersed in pure ethanol solution overnight. Densities of pure ethanol (ρ_{ETOH}), 0.789 g mL^{-1}, and PCL (ρ_{PCL}), 1.45 g cm^3, were used in subsequent calculations. Surface of samples was blotted dry and their mass was recorded to determine the amount of ethanol present within the sample. The porosity was calculated as follows:

$$\theta = V_{ETOH}/(V_{ETOH} + V_{PCL}) \quad (1)$$

$V_{ETH}$is the volume of intruded ethanol derived from the ratio between the observed change in mass after intrusion and ρ_{ETOH}. V_{PCL} denotes the volume of PCL fibers derived from a mass of a dry sample and ρ_{PCL}.

2.6. Mechanical tensile testing

Mechanical properties of scaffolds were measured under uniaxial tensile testing using an Advanced Rheometric Expansion System, ARES, rheometer (TA Instruments, New Castle, DE) with a normal force transducer range of 2–2000 g_f with 0.01% accuracy. Eight rectangular test specimens for each condition were prepared with a length of 50 mm, width of 5 mm. To minimize crack formation, the two ends of the specimens were sandwiched in

between molten sheets of PCL and clamped within fixtures. A schematic illustration is shown in Fig. S1. The initial length was recorded after loading of the specimen. A constant displacement rate of 10 mm/min was applied. Experimental data was collected and processed using TA Orchestrator software. The Young's modulus was calculated from the slope of the initial linear strain region of the stress-strain curve. Toughness (work to fracture) was measured as the area under the stress-strain curve from initial strain until fracture. Ultimate tensile strength was obtained from the stress-strain curves. Scaffold thickness was measured using SEM by mounting samples onto a 90 degree SEM mount. Three different scaffolds were used from each condition and 10 separate measurements were made for each sample.

2.7. Osteoblast proliferation on PCL-dECM scaffolds

Osteoblasts were expanded and seeded as stated above. After 24 hours of culture, the growth media was replaced with the osteogenic medium (αMEM supplemented with 0.1 μM dexamethasone, 0.05 mM ascorbic acid, and 10 mM glycerophosphate) (all from Sigma-Millipore). CellTiter 96® AQueous Non-Radioactive Cell Proliferation Assay (MTS) (Promega) was used to assess proliferation at days 7, 14, 21, and 28 of cultures. The assay was performed according to manufacturer's protocol. Five samples for each condition were used. Absorbance was measured at 490 nm after 2 h incubation using a microtiter plate reader (Synergy™ HT, BioTek Instruments, Inc.). Tissue culture plate (TCP) condition was used as a reference material/surface for evaluation of the effects of scaffolds on osteoblast growth characteristics, ALP activity, and mineral deposition. [51,52,53]

2.8. Alkaline Phosphatase (ALP) assay

ALP activity was measured in osteoblast cultures using a colorimetric ALP assay kit (Abcam, ab83369) according to the manufacturer's instructions. Briefly, samples were washed in cold PBS and lysed using 1 mL of assay buffer. Scaffolds were removed from coverslips, transferred to a 1.5 mL centrifuge tube with the cell lysate, and vortexed for 30 secs. Extracts were centrifuged at 13.5g for 15 min at 4 °C. Ten microliters of protein solution was added to 120 μL of working solution in a 96-well plate and incubated for 1h at 37°C. The reaction was halted by adding 20 μL of stop solution. The absorbance was measured at 405 nm. The p-nitrophenol concentration in samples was measured, correlated to standard concentrations, and normalized to the cell number (U/ml/cell). Five samples from each group were tested at each time point. TCP condition was used as a reference material for determining the effects of scaffolds on ALP activity [51,52].

2.9. Alizarin Red S (ARS) staining and quantification

Osteoblasts were stained with ARS for calcium deposits after 28 days of culture. Samples were rinsed with PBS, fixed in 4% paraformaldehyde solution for 30 min, and stained for 30 min with 2 mL of 40 mM ARS (Millipore, TMS-008-C) (pH=4.2) under gentle shaking. ARS was aspirated and wells were washed 5 times with H_2O for 5 mins to remove nonspecific staining. Red calcium deposits were captured using a Nikon T100 Stereomicroscope. TCP condition was used as a reference material/surface for evaluation of the effects of scaffolds on osteoblast mineral deposition. [51,52] For ARS staining quantification, dried samples were transferred into 1.5 mL centrifuge tubes and destained in

1 ml of 10% (w/v) cetylpyridinium chloride (CPC) 10mM sodium phosphate solution overnight at room temperature. The absorbance of samples measured at 562 nm. Sample concentration was determined by correlating measurements with a standard curve generated by serial dilution of ARS in CPC solution.

2.10. Immunostaining for OC and OPN

At day 28 of culture, osteoblast cultures were stained for bone mineralization markers, OC and OPN. Scaffolds were rinsed with PBS, fixed for 30 min in 4% paraformaldehyde solution, and permeabilized in 0.1% Triton X-100 in PBS for 20 mins under gentle agitation. Samples were blocked for 1 h in PBS containing 1% BSA. Blocking solution was used for all subsequent antibody incubations and washes. Samples were incubated in primary antibody solutions for OPN (Abcam, ab8448), or OC (ThermoFisher, MA1–82975) at dilutions 1:1000 and 1:500, respectively, overnight under gentle agitation at 4°C. After rinsing in the blocking solution three times for 10 minutes, secondary antibodies, Alexa Flour™ 488 and 594 (ThermoFisher, A11008 and A11005, respectively) were added at a 1:2000 dilution and incubated for 30 min at RT. After six washes, samples were mounted using Fluoroshield with DAPI (Sigma), observed using a fluorescence microscope (BZ-X710, Keyence) with the image software BZ-H3 (Keyence).

2.11. Cortical Bone Injury

A rat femoral cortical bone defect model was used to evaluate the regenerative capacity of PCL-dECM nanofibrous scaffolds *in vivo*. All animal procedures followed protocols approved by the Stevens Institute of Technology Institutional Animal Care and Use Committee and the NIH Guide for the Care and Use of Laboratory Animals. Adult male Sprague-Dawley rats (500g, male, Charles River Laboratories, Inc. Wilmington, MA) were anesthetized by inhalation of isoflurane using a VetEquip anesthesia system (VetEquipInc, Pleasanton, CA). The concentration of isoflurane was controlled at 2.0–3.0% and adjusted as needed to keep animals sedated with smooth breathing. A right hind leg was shaved and Betadine (West Chemicals Inc, Long Island, NY) was applied onto exposed skin. A 15-mm incision was made along the femoral axis. Fascia connecting biceps femoris and vastus lateralis was cut, the surrounding muscles were moved aside with blunt instruments, and the anterior femur was exposed using periosteal elevator. The initial hole was drilled on the distal side of the lesser trochanter of the femur with a 3-mm flat burr through the cortex into medullary cavity using a dental drill (RAM Rampower 35 Control Box with Tech2000 Handpiece, RAM Products, Inc., Dayton, NJ). A 5-mm flat burr was used to enlarge the defect. Sterile PBS was continuously sprayed into the defect to rinse the bone chips away and to minimize tissue damage. Each rat received a defect in the right femur. Eight defects per experimental group were available for analysis. Six groups of eight rats per group were assigned: (1) control, defects unfilled; defects covered with (2) PCL scaffolds; (3) COL scaffolds; (4) ENDO scaffolds; (5) OST scaffolds; and (6) EO scaffolds. Premade and disinfected rectangular scaffolds (10 mm length, 20 mm width) were rinsed with PBS and rolled over the defects. Fig. S2 shows a representative image of the implanted scaffold over a defect. Muscles were sutured using a continuous 5–0 suture. Skin wounds were closed with 4–0 vicryl discontinuous sutures. Following surgery, rats received subcutaneous injections of analgesic and were allowed to ambulate freely.

2.12. Histology and Histomorphometry

Animals from each group were sacrificed 6 weeks post-surgery. Femurs were dissected and fixed in 10% Neutral Buffered Formalin (Sigma) overnight. Tissue samples were decalcified in 10% EDTA/PBS solution, and dried in an ethanol series. Samples were embedded in a Technovit 7100 resin according to manufacturer's instructions. Samples were cut into 5–7μm thick longitudinal sections using a rotary microtome (Microm HM 360, Thermo Scientific) and mounted on Superfrost-plus slides (Fisher). For each sample, a total of 15 sections were cut across the injured area. Sections were stained with hematoxylin and eosin (H&E), Masson's Trichrome (MTC) and von Kossa (VK) stains.

Before each staining procedure, slides were immersed three times in xylenes solution for 5 minutes, followed by a series of ethanol washes to hydrate the slides: three times in 100% ethanol for 5 minutes, one time in 95% ethanol for 5 minutes, and 80% ethanol solution for 5 minutes, and in distilled water for 5 minutes. After staining, sections were dehydrated with two washes of 95% alcohol, two washes in absolute alcohol. All samples were clear in two washes of xylenes and mounted in Permount™ Mounting Medium (Electron Microscopy Sciences (EMS), #17986–01). For H&E staining [54], sections were immersed in Harris Hematoxylin solution (Sigma, HHS32) for 5 minutes and rinsed in deionized water for 5 minutes. Samples were quickly dipped three times into differentiation solution (Sigma, A3179) and rinsed in distilled water for 5 minutes. Samples were immersed in 1X Scott's Tap Water Substitute (Sigma, S5134) for 1 minute and later in 95% ethanol for 30 seconds. Sections were stained in Eosin Y Solution (Sigma, HT1101) for 1 minute. For MTC staining [55], slides were mordanted in preheated Bouin's Solution (EMS, 26367–01) for 1 hour at 56°C. After cooling, slides were rinsed in running tap water until yellow color was removed from sections. Slides were stained with a working Weigert's Iron Hematoxylin Solution (mix equal parts of Weigert's Iron Hematoxylin A (EMS, 2636702) and Weigert's Iron Hematoxylin B (EMS, 26367–03)) for 5 minutes and rinsed in distilled water. Samples were then stained in Biebrich Scarlet-Acid Fuchsin (EMS, 26367–04) for 15 minutes, followed by rinse in distilled water. Slides were immersed in Phosphomolybdic Acid-Phosphotungstic Acid (EMS, 26367–05) for 15 minutes and stained in Aniline Blue Solution (EMS, 26367–06) for 10 to 20 minutes. Sections were differentiated in Acetic Acid, 1% (EMS, 26367–07) for 3 to 5 minutes. For VK staining [56], sections were incubated in 1% silver nitrate solution (Sigma, 209139) under a 100 watt light bulb for 4 hours. Samples were rinsed in distilled water. Un-reacted silver was removed with 5% sodium thiosulfate (Sigma, 563188) for 5 minutes and followed by rinse in distilled water. Samples were counterstained with nuclear fast red (Sigma, 1.15939) for 5 minutes and rinsed in distilled water. Samples were imaged using brightfield settings (BZ-X710, Keyence). Bone histomorphometry was performed on sections using ImageJ software. Primary histomorphometry measurements taken were: area of bone formation per unit area, total perimeter of new bone formation per unit area, and cortical width. For each measurement, the images of 8 sections were used.

2.13. Statistical Analysis

Quantitative data is presented as sample mean ± standard deviation. The statistical significance was calculated using a one-way ANOVA in GraphPad Prism 6, and confirmed

with Tukey post-hoc test. A confidence interval of $p < 0.05$ was considered statistically significant.

3. RESULTS

3.1. Electrospun PCL and PCL-ECM nanofibers

The designation of top/bottom layers for *in vitro* experiments was made with consideration for *in vivo* implantation experiments. The study was designed with the hypothesis that the top layer (facing away from the femur) would aid in bone formation through osteogenic cues in osteoblast dECM. This layer (OST) was expected to be exposed to osteoblasts and bone lining cells in the periosteum, and that the osteogenic cues embedded in it, would facilitate osteoblast migration and closing of the defect via bone formation. In contrast, exposing endothelial dECM (as in ENDO/PCL) could have caused proliferation of fibroblasts, hinder formation of the bone around the defect, and result in fibrosis, since osteogenic cues would be absent in the top layer. The bottom layer (facing towards the surface of the bone) was meant to aid vascularization and indirectly enhance bone formation and through vascular cues in endothelial dECM. [57] The bottom layer was expected to be in contact with BMSCs, other osteoprogenitors as well as endothelial cells in the bone marrow. Positioning the layer with endothelial dECM would minimize its exposure to fibroblasts.

For *in vitro* experiments, the objective was to test the effectiveness of EO scaffold (OST/ENDO) in terms of bone formation and osteoblasts were cultured to this end. Due to tissue specificity, it was expected that osteoblasts would respond favorably to OST dECM; thus, in order to maximally expose osteoblasts to the layer with osteoblast dECM, osteoblasts were directly seeded onto OST layer (top layer). In a hypothetical ENDO/OST combination, osteoblasts would not be maximally exposed to osteogenic cues in the osteoblast dECM in the OST layer, since it would be partially masked by the ENDO layer. It was anticipated that osteoblasts would respond less favorably to the ENDO layer in ENDO/OST due to the tissue specificity. Therefore, this combination was excluded from the experimental design.

To control for any effects from release of dECM factors from the fibers in the bottom layer, the orientation of the fibers with respect to top/bottom was maintained and specific layers were substituted with PCL layer, which did not contain any cues. To control for the effect of osteoblast dECM in EO, the OST layer was substituted with the PCL and the ENDO layer remained underneath (PCL/ENDO). Conversely, to control for the release of any factors from endothelial dECM, the ENDO layer in EO was substituted with the PCL layer and the OST layer remained on top of the PCL layer (OST/PCL).

3.2. DNA and protein content evaluation of dECMs

The DNA and protein content determine effectiveness of decellularization. For qualitative assessment, decellularized EC and osteoblast cultures were stained with MB and CB. PCL fibers without any dECM were used as controls (Fig. S3A and D, respectively). MB staining (Fig. S3B and C, respectively) revealed small discernable structures. CB staining of EC cultures (Fig. S3E) had protein aggregates organized into extensive networks signifying tubulogenesis. CB stained osteoblast cultures (Fig. S3F) revealed scattered protein

aggregates that did not form any discernible structures. DNA content in EC and osteoblast cultures (Fig. S3G) was 16.63±5.97 and 12.64±4.84ng DNA/mg scaffold, respectively. There was a significant difference (P<0.0001) in protein content between EC and osteoblast cultures with 0.685±0.132mg and 3.252±0.072mg, respectively (Fig. S3H).

3.3. Fiber Morphology and Porosity

Fiber diameter decreased with the addition of dECM into the polymer solution, Fig. 2A–D. The mean fiber diameter for PCL fibers (Fig. 2I) was 1.109±0.215 μm and ranged from 0.564μm to 1.901μm. Fibers with embedded dECM had a significantly reduced fiber diameter, 0.468± 0.127μm for COL fibers, 0.123±0.056μm for ENDO fibers, and 0.118±0.047μm for OST fibers. Fig. 2E–H shows the fiber diameter distribution for each condition. For COL group fibers ranged from 0.153μm to 1.148μm. Addition of globular protein in dECM reduced the propensity to form thick fibers with diameter range from 38nm to 430nm for ENDO and 47nm to 368 nm for OST groups. Solutions with dECM also formed large beads. The average pore size in the mesh layers was reduced from 0.434±0.618 μm^2 in PCL group to 0.186±0.262μm^2 for COL, 0.047± 0.063 μm^2 for ENDO, and 0.034±0.032 μm^2 for OST (Fig. S4A–E). However, the porosity of the scaffolds did not significantly change with the addition ofdECM to the polymer solution. Porosities (Fig. 2J) were calculated as follows: 87.99± 2.34% for PCL fibers, 88.01±3.25% for COL, 88.05±6.11% for ENDO, 83.34± 1.39% for OST, and 82.98± 8.27% for EO.

3.4. Mechanical tensile testing

Scaffold thickness was measured to calculate the cross sectional area and there was no statistical difference between ENDO and OST fibers nor between COL and EO fibers (Fig. S5). Tensile strength (Fig 3A) for the PCL condition represents the highest stress recorded, 1.015±0.067 MPa. Unlike other samples, PCL samples did not fracture. In other conditions, tensile strength was recorded when one of the layers of the scaffolds ruptured. The tensile strength in the COL condition, 11.618±1.837 MPa, indicates that addition of fibrous protein into polymeric fibers can enhance their strength. Addition of globular dECM protein in ENDO, OST, and EO conditions did not provide such reinforcement. Similar trends could be observed in the measurement of Young's modulus (Fig. 3B) and yield stress (Fig. 3C). Embedding globular dECM protein into fibers caused them to rupture more readily than PCL and COL fibers as evidenced by an order of magnitude difference in toughness (Fig 3D).

3.5 In Vitro cell responses to PCL-dECM fibers

3.5.1 Osteoblast and EC attachment—Bioactivity of PCL-dECM fibers can be evidenced in attachment characteristics of cells. Fig. 4 A–E shows morphology change in ECs upon attachment to different fiber surfaces. In Fig. 4A and C, where the top layer is PCL fibers, ECs attach mainly at the fiber junctions and retain a rounded morphology. ECs spread on fibers with embedded dECM, (Fig 4B, D, E). In EO condition, fewer cells are rounded than in the other two conditions, indicating that the bottom layer with embedded EC dECM might have been sensed by cells. Osteoblasts showed phenotypic change, Fig. 4 F–J. In PCL, COL, and ENDO conditions, osteoblasts had a bone-lining phenotype, Fig. 4F–H.

In OST and EO conditions, with osteoblast dECM embedded in the top layer, their morphology became cuboidal, Fig. 4I–J.

3.5.2 Proliferation—Fig. 4K shows proliferation of rat osteoblasts on fibrous scaffolds in differentiation media. The difference between TCP and fiber cultures could be attributed to greater surface area available for cell attachment. In the first two weeks of culture, there was no statistical difference in growth between groups. At day 21, there was a significant difference in cell number values between PCL ($p<0.01$) and COL ($p<0.001$) scaffolds and ENDO, OST, and EO scaffolds. Cell number values for PCL and COL scaffolds were $1.634\pm0.122 \times10^6$ and $1.482\pm0.129\times10^6$ cells, respectively. Cell number values for ENDO, OST, and EO were $1.846\pm0.194\times10^6$, $1.883\pm0.256\times10^6$, and $1.928\pm0.066\times10^6$ cells, respectively. This suggests that embedding dECM protein in the polymeric fibers enhanced their proliferation and that this effect may take up to 21 days. At day 28, the modest increase in absorbance values in ENDO, OST, and EO groups indicates that cultures might have reached their growth plateau.

3.5.3 ALP—On Day 14, osteoblasts grown on ENDO scaffolds had a significantly higher ALP activity ($p<0.001$) than other scaffolds with embedded dECM, Fig. 4L. After 21 days, ALP activity in PCL, ENDO, and TCP condition remained significantly higher than COL, OST, and EO conditions. The corresponding values for ALP activity for cultures on these scaffolds were, $6.295\pm0.326\times10^{-6}$, $4.780\pm0.347\times10^{-6}$, $5.288\pm0.582\times10^{-6}$, $2.438\pm1.864\times10^{-6}$, $3.826\pm1.236\times10^{-6}$, and $7.407\pm0.878\times10^{-6}$ U/ml/cell for PCL, COL, ENDO, OST, EO, and TCP, respectively. At day 28, ALP activity in COL and dECM groups was lower than in PCL and TCP groups. Based on these results, embedding of dECM did not translate into higher activation of ALP enzyme.

3.5.4 ARS Staining and Quantification—Osteoblast cultures were stained with ARSto compare mineralization levels after 28 days of culture, Fig. 5. In TCP condition, stained nodules were grouped in the center of the culture well, Fig. 5F. In PCL (Fig. 5A,G), COL (Fig. 5B,H), and ENDO (Fig. 5C,I) groups, similar levels of staining were observed with about half of the scaffold stained pink-red color. OST and EO conditions, Fig. 5D,J and E,K respectively, had pronounced dark red staining, with OST scaffold entirely covered in dark red stain. Quantification, Fig. 5L, confirmed that OST scaffold had a significantly greater ARS concentration, 1.400±0.604mM compared to other conditions, and no significant difference between other conditions.

3.5.5 OC and OPN—To confirm results from ARS experiments, cultures were stained with OC and OPN mineralization markers after 28 days, Fig. 6. The presence of extracellular OPN was pronounced in OST group (Fig. 6N, P, X) and to a lesser extent in COL culture (Fig. 6F, H, V). In PCL (Fig. 6B, D,U) condition, OPN was secretedthroughout the culture in select regions. In ENDO (Fig. 6J, L,W) and EO (Fig. 6R,T,Y), both conditions with EC dECM, OPN was localized mostly intracellularly. OC staining did not provide a clear indication of a difference in secretion levels between PCL (Fig. 6C), COL (Fig. 6G), OST (Fig. 6O), or EO (Fig. 6S) conditions. ENDO condition (Fig. 6K) appeared to have the

fewest cells stained positively for OC. DAPI staining (Fig. 6A,E,I,M, Q) was used to distinguish intracellular and extracellular deposits.

3.6 Histology and Histomorphometry

The histology of femur sections revealed all defects healed to varying degrees, Fig. 7A–F and Fig. S6. Scaffolds did not rupture under shear stress from the muscle, but some were enveloped and displaced by the muscle. The regenerated bone area as a ratio of the total defect area (Fig. 7G) in experimental groups regardless of the fiber composition was a significantly greater ($p<0.01$) than in the control group. In defect group, the ratio of area of newly formed bone to total area of defect was0.296±0.070,and in PCL, COL, ENDO, and OST groups the ratios were 0.468±0.060, 0.465±0.059, 0.454±0.058, and 0.451±0.093, respectively. In EO condition, the ratio was 0.474±0.080, ($p<0.001$). There was no significant difference in the perimeter of the newly formed bone tissue among groups (Fig. 7H). However, the cortical width at the center of a defect (Fig. 7C) was a significantly greater ($p<0.0001$) in EO condition, 301.95±76.27μm,compared to other groups, 186.20±55.21μm (Defect), 174.95 ± 29.22 μm (PCL), 147.06 ± 31.65 μm (COL), 162.21±34.73 μm (ENDO), 154.60±52.33 μm (OST).

4. DISCUSSION

Embedding dECM into polymeric nanofibers presents a strategy for mimicry of the bone microenvironment by biosynthetic grafts. The dECM contains a tissue-specific array of bioactive protein, carbohydrates, and their genetic variants that is difficult to replicate with sequential surface modifications. [58,59] The approach presented here allows for inclusion of less known components of bone ECM and optimization of the fiber composition by combining multiple dECMs. Fibers also provide contact guidance cues to orient cells, and their high surface to volume ratio regulates presentation, release, and degradation of dECM.

The goal of this study was to fabricate bioactive nanofibrous PCL-dECM scaffolds with embedded osteogenic and vascular cues for regeneration of large bone defects. To present cell-derived dECMs from primary rat osteoblasts and ECs on the surface of fibers, PCL-dECM solutions were sequentially electrospun as two connected layers. The scaffold design aimed to enhance bone formation on the top surface of the scaffold and increase vascularization in the inner part of the defect. The purpose of embedding dECMs was to functionalize PCL fibers with protein epitopes, not necessarily the entire protein. A protein may not retain its entire tertiary and quaternary structure after it has been removed from of its aqueous environment and placed in an organic solvent, such as HFIP. However, some of the protein functional epitopes remained exposed after embedding, provided a diverse source of chemical and biological signals to the attached cells, and bound growth factors released during clotting. Moreover, as the polymer degraded and more of the protein became exposed, more epitope signals were revealed and some protein were released into the microenvironment. We predicted that the scaffold with these osteoconductive and vascular stimuli would enhance bone growth. To verify this, scaffolds were evaluated *in vitro* and showed enhanced osteoblast proliferation and mineralized matrix deposition. To assess the validity of our approach *in vivo*, scaffolds were implanted in a rat cortical bone defect.

PCL-dECM scaffolds overcome a drawback of synthetic scaffolds by providing crucial morphogenic cues on their surface. Histomorphology indicated that physical guidance cues provided by fibers may aid in formation of the nascent bone by serving as a migratory bridge for osteoblasts and stem cells. Similar mechanism underlies the concept of Masquelet technique that takes advantage ofa biomembrane encapsulating a cement spacer [60]. Scaffolds also blocked infiltration of other endogenous cells into the defect and prevented pseudoarthrosis. The embedded protein did not elicit an immune response or fibrosis, although some scaffolds were displaced by a growing surrounding tissue.

Similarly, studies by other groups demonstrated the effectiveness of dECMs for enhancement of bone regeneration. Scaffolds prepared from dECM of porcine cancellous bone increased expression of OC and OPN and supported MSC differentiation in vitro. In the rabbit femoral condyle defect model, dECM scaffolds with low stiffness had significantly increased deposition of ECM and mature bone matrix. Moreover, low stiffness dECM scaffolds had significantly reduced fiber capsule thicknesses, a gap between bone and a scaffold, attenuated in vivo inflammatory response, and increased the number of vascular structures compared to the control group. [61] In another study, adipose tissue dECM hydrogel implanted into mouse critical-sized femoral defects resulted in significantly increased expression of collagen and osteopontin, bone volume, bone area, and overall amount of regenerated tissue after 6 weeks relative to the untreated group. [62] Likewise, dECM scaffolds derived from small intestinal submucosa had increased bone formation ratio and bone mineral ratio 4 and 8 weeks post-implantation into mouse calvarial defects. [63]

Other groups produced polymer-dECM fibers for bone regeneration and evaluated these constructs *in vitro*. Coating polymeric fibers with ECMs by directly culturing cells on fibers [36,37] constrains the available surface for dECM deposition and the final amount of isolated dECM. It also renders dECM prone to degradation after implantation. Embedding tissue-derived dECM nanoparticles into PCL fibers can be an efficient method for composite fiber production, but protein of animal origin introduce a risk of immune response and an inherent composition variability that is difficult to control. [8] Cell-derived dECMs from co-cultures might result in limited or altered dECMs from one or both phenotypes [18]. Here, separate cultures bypass mixing of media as VEGF supplement in EC media may alter osteoblast and undifferentiated MSCs phenotype. Primary osteoblasts were chosen as they are more prone to releasing nascent bone ECM components than undifferentiated MSCs.

The discrepancy between *in vitro* and *in vivo* results indicates that cooperation between different cell phenotypes *in vivo* introduces extraneous factors that need to be considered when evaluating bone scaffolds. Similarly to other *in vitro* studies, tissue specificity of the dECM was evident. [18,21] Osteoblast proliferation, mineralization, and OPN secretion were mostly enhanced in OST group despite an identical top layer in EO group. Differences in attachment phenotype and mineralization between OST and EO groups indicate that the surface of fibers degraded and released embedded EC dECM factors from the bottom layer not in contact with the cells. ECs have been shown to inhibit or delay bone calcification *in vitro*. [64] However, released EC protein may not contribute to osteoblast mineralization *in vitro*, but may indirectly stimulate other cells to contribute to this process by supporting osteoblast maturation. This could account for the differences in cortical width *in vivo*. EC

dECM contains collagen type IV, laminin isoforms, heparan sulfate sulfate proteoglycans (perlecan and agrin), and nidogens. [65] Exposed epitopes of these protein and carbohydrates can provide direct signaling via integrin binding to osteoblasts, BMSCs, osteoprogenitors. For example, laminins, a major component of endothelial ECM transducing signals that control cell migration, survival, proliferation, and differentiation. In response to this signaling, these osteogenic cells can proliferate, differentiate, or secrete a series of growth factors to stimulate vascularization (vascular endothelial growth factor, VEGF) and migration into the defect (transforming growth factor beta, TGFβ). In response to this VEGF secretion, endothelial progenitor cells can secrete BMPs 2,4 and 7 causing osteoprogenitor migration, differentiation, and further increase in VEGF secretion, thus initiating a positive feedback loop. [66] Stimulation of endothelial progenitor cells in bone marrow via integrin binding can also lead to secretion of other growth factors such as insulin-like growth factor (IGF) or TGFβ. [67,68] Equally likely, the increased growth by cells infiltrating the defect in EO samples can be attributed to increased affinity to bind growth factors by the exposed dECM epitopes. Laminins, heparan sulfate proteoglycans, and multiadhesive glycoprotein found in endothelial dECM can sequester the above-mentioned growth factors and morphogens with their surface receptors. These growth factors when released during clotting can activate proliferation of endothelial cells or differentiation of osteoprogenitors resulting in bone formation response. [69]

Differences in proliferation in ENDO, OST, and EO groups appeared after 21 days of culture and reached a plateau after 28 days. Cultures on larger constructs over a longer period of time may be necessary to elicit similar effects on osteoblasts as observed i*n vivo* 6 weeks post-implantation. Conversely, it is possible that insufficient amount of dECM was exposed on the fibers to elicit an early measurable difference in proliferation. Despite on-going studies, the therapeutic amount of dECM to be embedded into fibers and its composition have yet to be determined. Other groups embedded 0.025–10% (w/w) of dECM, but perhaps greater concentrations are required to achieve robust bone growth. One of the objectives of this study was to present a maximal amount of dECM on the surface of fibers, since high polymer concentrations may mask majority of bioactive epitopes. Concentration of PCL was gradually increased and parameters were optimized until a solution yielded fibers and minimized bead formation.

Solubility of the dECM poses a challenge as charged groups conflict with nonpolar polymers. To resolve this, dECMs were dissolved in HFIP/formic acid/DMSO. Although HFIP leads to undesirable degradation of protein structures [70,71], the results indicate that some bioactivity of dECMs was preserved. Embedded osteoblast dECM in OST and EO groups altered morphology of osteoblasts upon attachment to cuboidal phenotype. Differences in fiber diameter between groups present a plausible alternative explanation to the morphological changes rather than fiber composition. [72] However, in COL group, osteoblasts retained the flat bone lining morphology as in PCL group despite differences in fiber diameter.

Addition of dECM into PCL solution decreased fiber diameter and reduced average pore size in PCL-dECM groups. Embedded collagen and dECM in the fibers increased their tensile strength, Young’s modulus, yield stress, and toughness. The comparison of the results

between COL and ENDO, OST, and EO samples revealed that the structure of protein has influence on the strength of the fibers. Fibrous collagen in COL samples enhanced the strength of the fibers likely because individual collagen fibers aligned with the polycaprolactone chains as fibers began to form during electrospinning. Amino acid residues in collagen could form electrostatic interactions between carboxyl groups in polycaprolactone, which would require additional energy (force) to pull these chains apart and fracture the sample. Globular protein in dECM did not align with the polycaprolactone chains, likely disrupting their alignment in a PCL fibers, and introduced structural defects into the molecular structure of a fiber. The increase in mechanical properties in ENDO, OST, and EO samples resulted from the additional energy required to separate interactions between amino acid residues in dECM that and carboxyl groups in PCL as well as those between amino acid residues within that maintained the globular conformation of the protein. The additional energy required to “untangle” the globular protein probably contributed to the increased strength of the fibers. As a result, EO sample with both layers having embedded dECM required more energy to fracture than either OST or ENDO sample.

The overall porosity of scaffolds was not affected. In all groups, the calculated porosity was greater than 80%, and similar results were previously noted. [50,73,74] However, with the average pore size less than 1μm^2, cell penetration through the nanofibrous matrix was greatly thwarted [75], as evidenced by limited presence of cells within the scaffold after implantation. Thus, fibrous scaffolds may be more influential in enhancing the initial cell attachment, providing guidance cues, aligning cells and their matrix in a specific orientation, and releasing mineralization cues. [9]

Controlling presentation of a specific amount of the dECM on a scaffold surface remains to be a challenge. A dose response study can determine the optimal molecular composition and the amount of dECM for osteoblast mineralization. There is evidence that a mineralized matrix containing greater quantities of calcium and collagen may induce a more robust osteogenic response [76]. As one study suggests, amount of mineral deposition may correspond in a dose-dependent manner to the protein concentration within dECM. [77] Combining multiple dECMs will introduce a subsequent challenge in determining which dECM combinations and their respective amounts are therapeutic. Some dECM combinations might alter endogenous cells infiltrating the graft towards cartilage formation or fibrosis. Not all dECM combinations will be therapeutic [21]. Osteoblast dECM alone may not be optimal in heterogeneous bone microenvironment; thus, other dECM combinations should be investigated.

The study had some limitations that warrant further investigation. Osteoblast cultures were supplemented with an artificial osteogenic cocktail, which may not accurately simulate *in vivo* microenvironment. Given that several cell types regulate bone growth in concert with osteoblasts, the osteogenic media may inadequately stimulate osteoblasts or mask secondary effects of dECMs. Likewise, exclusion of these cells from osteoblast culture likely contributed to the discrepancies with *in vivo* results. Early and late time-points in the *in vivo* study can provide insights into the healing response of the cortical injury and the initial cellular response to the implant.

To take advantage of this technology and arrive at a clinically relevant construct, future studies require optimization to accommodate compressive stresses in segmental defects. This may include increasing a number of layers in the scaffold and altering its geometry to prevent displacement by the growing tissue. Alignment of polymeric fibers across the defect may better guide cells across the gap, increase their migration, and result in secretion of an aligned matrix similar to collagen fibrils in the bone. [78]

In summary, the results of this study demonstrate the potential of polymer-dECM scaffolds to mimic bone native micro-environment and accelerate bone healing. Embedding dECM into polymeric fibers provides a modular platform that can be optimized to enhance osteoblast attachment and proliferation, while restricting access of other phenotypes that disrupt bone formation during healing process. This study improves material properties of synthetic polymers by introducing a novel method of fabrication of biologically responsive biomaterials for bone defect regeneration.

5. CONCLUSION

Combination of synthetic polymers and cell-secreted dECMs presents a novel design for engineering biosynthetic bone graft that mimic bone microenvironment and augment bone's capacity to regenerate. This study evaluated an efficient method for fabrication of dual-layer polymer-dECM scaffolds with embedded osteogenic and vascular cues from osteoblast and EC dECMs. Scaffolds were evaluated as a substrate in an osteoblast culture and in a cortical bone defect of a rat femur. The study demonstrates changes in mechanical properties upon dECM embedding, retention of its bioactivity, and increased cortical bone growth after implantation. Scaffolds with embedded osteoblast dECM enhanced osteoblast proliferation and mineral deposition in tissue specific manner. However, histomorphological analysis of cortical bone sections showed that osteogenic and vascular cues stimulate bone growth to a greater extent than either of the cues alone. Main advantages of the biocomposite nanofibrous scaffold design are ease of fabrication, malleability of fiber composition, and physical guidance provided by fibers that may prove to be critical in healing of an injured bone. The results of the study illustrate the potential of nanofibrous polymer-dECM scaffolds to aid regeneration of bone defects by presenting dECM cues that recapitulate bone ultrastructure. This concept of biomimicry through biocomposite fibers may prove advantageous in future tissue engineering designs to produce clinically relevant constructs for bone regeneration.

Supplementary Material

Refer to Web version on PubMed Central for supplementary material.

Acknowledgments

The work was partly supported by the Assistant Secretary of Defense for Health Affairs, through the Peer Reviewed Medical Research Program under Award No. W81XWH-16-1-0132, and the National Institute of Biomedical Imaging and Bioengineering of the National Institutes of Health (award number R01EB020640). We would like to thank Dr. George McConnell for his generous access to the BZ-X710 fluorescence microscope.

REFERENCES

1. Tzioupis C, Giannoudis PV, Prevalence of long-bone non-unions. Injury 38(2007) S3–9.
2. Boden SD, Biology of lumbar spine fusion and use of bone graft substitutes: present, future, and next generation. Tissue Eng. 6 (2000) 383–399. [PubMed: 10992434]
3. Green E, Lubahn JD, Evans J, Risk factors, treatment, and outcomes associated with nonunion of the midshafthumerus fracture. J SurgOrthop Adv. 14 (2005) 64–72.
4. Tour G, Wendel M, Tcacencu I, Cell-Derived Matrix Enhances Osteogenic Properties of Hydroxyapatite, Tissue Eng Part A. 179 (2011) 127–137.
5. Rihn JA,Kirkpatrick K, Albert TJ, Graft options in posterolateral and posterior interbody lumbar fusion. Spine 35 (2010) 1629–1639. [PubMed: 20628336]
6. Clough BH, McCarley MR, Krause U, Zeitouni S, Froese JJ, McNeill EP, Chaput CD, Sampson HW, Gregory CA, Bone regeneration with osteogenically enhanced mesenchymal stem cells and their extracellular matrix proteins. J Bone Miner Res. 30 (2015) 83–94. [PubMed: 25130615]
7. Marks SC, Odgren PR, Structure and Development of Skeleton, in: Bilezikian JP, Raisz LG, Rodan GA (Eds.) Principles of Bone Biology, Academic Press, San Diego, 2002, pp. 3–4.
8. Gibson M, Beachley V, Coburn J, Bandinelli PA, Mao HQ, Elisseeff J, Tissue extracellular matrix nanoparticle presentation in electrospun nanofibers. Biomed. Res. Int 2014 (2014) 469120. [PubMed: 24971329]
9. Huang G, Li F, Zhao X, Ma Y, Li Y, Lin M, Jin G, Lu TJ, Genin GM, Xu F, Functional and Biomimetic Materials for Engineering of the Three-Dimensional Cell Microenvironment. Chem Rev 117 (2017) 12764–12850. [PubMed: 28991456]
10. Gilbert TW, Stolz DB, Biancaniello F, Simmons-Byrd A, Badylak SF, Production and characterization of ECM powder: Implications for tissue engineering applications. Biomaterials 26 (2005) 1431–1435. [PubMed: 15482831]
11. Kim IG, Hwang MP, Du P, Ko J, Ha CW, Do SH, Park K, Bioactive cell-derived matrices combined with polymer mesh scaffold for osteogenesis and bone healing. Biomaterials 50 (2015) 75–86. [PubMed: 25736498]
12. Thibault RA, Mikos AG, Kasper FK. Scaffold/Extracellular Matrix Hybrid Constructs for Bone Tissue Engineering. AdvHealthc Mater. 2 (2013) 13–24.
13. Dennis SC, Berkland CJ, Bonewald LF, Detamore MS, Endochondral ossification for enhancing bone regeneration: converging native extracellular matrix biomaterials and developmental engineering in vivo. Tissue Eng Part B Rev. 21 (2015) 247–266. [PubMed: 25336144]
14. Kim HJ, Kim UJ, Vunjak-Novakovic G, Min BH, Kaplan DL, Influence of macroporous protein scaffolds on bone tissue engineering from bone marrow stem cells. Biomaterials 26 (2005) 4442–4452. [PubMed: 15701373]
15. Datta N, Holtorf HL, Sikavitsas VI, Jansen JA, Mikos AG, Effect of bone extracellular matrix synthesized in vitro on the osteoblastic differentiation of marrow stromal cells, Biomaterials 26 (2005) 971–977. [PubMed: 15369685]
16. Zeitouni S, Krause U, Clough BH, Halderman H, Falster A, Blalock DT, Chaput CD, Sampson HW, Gregory CA, Human mesenchymal stem cell-derived matrices for enhanced osteoregeneration. Sci Transl Med. 4 (2012) 132–155.
17. Thibault RA, Baggett LS, Mikos AG, Kasper FK, Osteogenic differentiation of mesenchymal stem cells on pregenerated extracellular matrix scaffolds in the absence of osteogenic cell culture supplements. Tissue Eng Part A. 16 (2010) 431–440. [PubMed: 19863274]
18. Carvalho MS, Silva JC, Udangawa RN, Cabral JMS, Ferreira FC, da Silva CL, Linhardt RJ, Vashishth D, Co-culture cell-derived extracellular matrix loaded electrospun microfibrous scaffolds for bone tissue engineering. Mater Sci Eng C. 99 (2019) 479–490.
19. Lau TT, Lee LQP, Vo BN, Su K, Wang DA, Inducing ossification in an engineered 3D scaffold-free living cartilage template.Biomaterials 33 (2012) 8406–8417. [PubMed: 22925815]
20. Bracaglia LG, Fisher JP, Extracellular matrix-based biohybrid materials for engineering compliant, matrix-dense tissues. Adv. Healthc. Mater 4 (2015) 2475–2487. [PubMed: 26227679]

21. Hong Y, Huber A, Takanari K, Amoroso NJ, Hashizume R, Badylak SF, Wagner WR, Mechanical properties and in vivo behavior of a biodegradable synthetic polymer microfiber-extracellular matrix hydrogel biohybrid scaffold. Biomaterials 32 (2011) 3387–3394. [PubMed: 21303718]
22. Narayanan G, Vernekar VN, Kuyinu EL, Laurencin CT. Poly (Lactic Acid)-Based Biomaterials for Orthopaedic Regenerative Engineering. Adv Drug Deliv Rev. 107 (2016) 247–276. [PubMed: 27125191]
23. Ghassemi T,Shahroodi A, Ebrahimzadeh MH, Mousavian A, Movaffagh J, Moradi A,Current Concepts in Scaffolding for Bone Tissue Engineering. Arch Bone Jt Surg. 6 (2018) 90–99. [PubMed: 29600260]
24. Kao ST, Scott DD, A review of bone substitutes. Oral MaxillofacSurgClin North Am. 19 (2007) 513–521.
25. Li Z, Tuffin J, Lei IM, Ruggeri FS, Lewis NS, Gill EL, Savin T, Huleihel L, Badylak SF, Knowles T, Satchell SC, Welsh GI, Saleem MA MA, Huang YYS, Solution fibre spinning technique for the fabrication of tuneabledecellularised matrix-laden fibres and fibrous micromembranes. Acta Biomater. 78 (2018) 111–122. [PubMed: 30099199]
26. Lu P, B Ding B Applications of electrospun fibers. Recent Pat Nanotechnol, 2 (2008) 169–182. [PubMed: 19076051]
27. Zhang G, Hawks SA, Ngo C, Schelhas LT, Scholes DT, Kang H, Aguirre JC, Tolbert SH, Schwartz BJ, Extensive Penetration of Evaporated Electrode Metals into Fullerene Films: Intercalated Metal Nanostructures and Influence on Device Architecture. ACS Applied Materials & Interfaces, 7 (2015) 25247–25258. [PubMed: 26488157]
28. Reznikov N, Shahar R, Weiner S, Bone hierarchical structure in three dimensions. Acta Biomater. 10 (2014) 3815–3826. [PubMed: 24914825]
29. Huang ZM, Zhang YZ, Kotaki M, Ramakrishna S, A review on polymer nanofibers by electrospinning and their applications in nanocomposites. Compos. Sci. Technol, 63 (2003) 2223–2253.
30. Gao S, Guo W, Chen M, Yuan Z, Wang M, Zhang Y, Liu S, Xi T, Guo Q, Fabrication and characterization of electrospun nanofibers composed of decellularized meniscus extracellular matrix and polycaprolactone for meniscus tissue engineering. J. Mater. Chem. B 5(2017) 2273–2285. [PubMed: 32263618]
31. Tzaphlidou M, The role of collagen in bone structure: an image processing approach. Micron 36 (2005) 593–601. [PubMed: 16209926]
32. DalleCarbonare L, Giannini S, Bone microarchitecture as an important determination of bone strength. J. Endocrinol. Invest 27(2004) 99–105. [PubMed: 15053252]
33. Hajiali H, Shahgasempour S, Naimi-Jamal MR, Peirovi H, Electrospun PGA/gelatin nanofibrous scaffolds and their potential application in vascular tissue engineering. Int J Nanomedicine 6 (2011) 2133–2141. [PubMed: 22114477]
34. Neves NM, Campos R, Pedro A, Cunha J, Macedo F, Reis RL, Patterning of polymer nanofiber meshes by electrospinning for biomedical applications. Int J Nanomedicine 2 (2007) 433–438. [PubMed: 18019842]
35. Jeon HJ, Lee JY, Lee H, Kim GH, Nanostructured surface of electrospun PCL/DECM fibres treated with oxygen plasma for tissue engineering. RSC Adv. 6(2016) 32887–32896.
36. Fu Y, Liu L, Cheng R, Cui W, ECM decorated electrospun nanofiber for improving bone tissue regeneration. Polymers 10 (2018) 272.
37. Young BM, Shankar K, Allen BP, Pouliot RA, Schneck MB, Mikhaiel NS, Heise RL, Electrospun decellularized lung matrix scaffold for airway smooth muscle culture. ACS Biomater. Sci. Eng, 3 (2017) 3480–3492.
38. Gao S, Chen M, Wang P, Li Y, Yuan Z, Guo W, Zhang Z, Zhang X, Jing X, Li X, An electrospun fiber reinforced scaffold promotes total meniscus regeneration in rabbit meniscectomy model. Acta Biomater. 73 (2018) 127–140. [PubMed: 29654991]
39. Baiguera S, Del Gaudio C, Lucatelli E, Kuevda E, Boieri M, Mazzanti B, Bianco A, Macchiarini P, Electrospun gelatin scaffolds incorporating rat decellularized brain extracellular matrix for neural tissue engineering. Biomaterials 35 (2014) 1205–1214. [PubMed: 24215734]

40. Yu H, VandeVord PJ, Mao L, Matthew HW, Wooley PH, Yang SY. Improved tissue-engineered bone regeneration by endothelial cell mediated vascularization. Biomaterials 30 (2009) 508–517. [PubMed: 18973938]
41. Li H H, Xue K K, Kong N, Liu K K, Chang J . Silicate bioceramics enhanced vascularization and osteogenesis through stimulating interactions between endothelia cells and bone marrow stromal cells. Biomaterials 35 (2014) 3803–3818. [PubMed: 24486216]
42. Xu Y, Wu Z, Donga X, Li H. Combined biomaterial signals stimulate communications between bone marrow stromal cell and endothelial cell. RCS Advances 7 (2017) 5306–5314.
43. Inglis S, Kanczler JM, Oreffo ROC. 3D human bone marrow stromal and endothelial cell spheres promote bone healing in an osteogenic niche. FASEB J 33 (2019) 3279–3290. [PubMed: 30403537]
44. Leszczak V, Place LW, Franz N, Popat KC, Kipper MJ, Nanostructured Biomaterials from Electrospun Demineralized Bone Matrix: A Survey of Processing and Crosslinking Strategies. ACS Appl. Mater. Interfaces 6 (2014) 9328–9337. [PubMed: 24865253]
45. Junka R, Yu X, Novel Acellular Scaffold Made from Decellularized Schwann Cell Sheets for Peripheral Nerve Regeneration, Regen EngTransl Med. 1 (2015) 22–31.
46. Johnson KM, Hanekamp T, Stayton MM. Methylene blue: an alternative, multi-purpose stain for detection, analysis and isolation of nucleic acids. Biopolym. Cell 13 (1997) 250–253.
47. Ray KJ, Simard MA, Larkin JR, Coates J, Kinchesh P, Smart SC, Higgins GS, Chappell MA, Sibson NR. Tumor pH and Protein Concentration Contribute to the Signal of Amide Proton Transfer Magnetic Resonance Imaging. Cancer Res 79 (2019) 1343–1352. [PubMed: 30679178]
48. Coronado RE, Somaraki-Cormier M, Natesan S, Christy RJ, Ong JL, Halff GA. Decellularization and Solubilization of Porcine Liver for Use as a Substrate for Porcine Hepatocyte Culture: Method Optimization and Comparison. Cell Transplant 26 (2017) 1840–1854. [PubMed: 29390876]
49. Schmitt A, Csiki R, Tron A, Saldamli B, Tübel J, Florian K, Siebenlist S, Balmayor E, Burgkart R. Optimized protocol for whole organ decellularization. Eur J Med Res 22 (2017) 31. [PubMed: 28886732]
50. Soliman S, Sant S, Nichol JW, Khabiry M, Traversa E, Khademhosseini A. Controlling the porosity of fibrous scaffolds by modulating the fiber diameter and packing density. J Biomed Mater Res A 96 (2011) 566–574. [PubMed: 21254388]
51. Nukavarapu SP, Kumbar SG, Brown JL, Krogman NR, Weikel AL, Hindenlang MD, Nair LS, Allcock HR, Laurencin CT. Polyphosphazene/nano-hydroxyapatite composite microsphere scaffolds for bone tissue engineering. Biomacromolecules 9 (2008) 1818–1825. [PubMed: 18517248]
52. Hosseini FS, Soleimanifar F, Ardeshirylajimi A, Vakilian S, Mossahebi-Mohammadi M, Enderami SE, Khojasteh A, Zare Karizi S. In vitro osteogenic differentiation of stem cells with different sources on composite scaffold containing natural bioceramic and polycaprolactone. Artif Cells Nanomed Biotechnol 47 (2019) 300–307. [PubMed: 30688102]
53. Bélanger MC, Marois Y. Hemocompatibility, biocompatibility, inflammatory and in vivo studies of primary reference materials low-density polyethylene and polydimethylsiloxane: a review. J Biomed Mater Res 58 (2001) 467–477. [PubMed: 11505420]
54. Gamble M, The Hematoxylins and Eosin, in: Bancroft JD, Gamble M (Eds), Theory and Practice of Histological Techniques, Churchill Livingstone, New York, 2002, pp. 121–134.
55. Sheehan D, Hrapchak B, Theory and Practice of Histotechnology, second ed., Battelle Press, Ohio, 1980, pp 189–190.
56. Sheehan D, Hrapchak B, Theory and Practice of Histotechnology, second ed., Battelle Press, Ohio, 1980, pp 226–227.
57. Witjas FMR, van den Berg BM, van den Berg CW, Engelse MA, Rabelink TJ, Concise Review: The Endothelial Cell Extracellular Matrix Regulates Tissue Homeostasis and Repair. Stem Cells Transl Med. 8 (2019) 375–382. [PubMed: 30537441]
58. Benders KE, van Weeren PR, Badylak SF, Saris DB, Dhert WJ, Malda J, Extracellular matrix scaffolds for cartilage and bone regeneration, Trends Biotechnol. 31 (2013) 169–176. [PubMed: 23298610]

59. Lin H, Yang G, Tan J, Tuan RS, Influence of decellularized matrix derived from human mesenchymal stem cells on their proliferation, migration and multi-lineage differentiation potential. Biomaterials 33 (2012) 4480–4489. [PubMed: 22459197]
60. Masquelet A, Kanakaris NK, Obert L, Stafford P, Giannoudis PV, Bone Repair Using the Masquelet Technique.J Bone Joint Surg Am. 101 (2019) 1024–1036. [PubMed: 31169581]
61. Hu Q, Hu Q, Liu M, Chen G, Xu Z, Lv Y, Demineralized Bone Scaffolds with Tunable Matrix Stiffness for Efficient Bone Integration. ACS Appl. Mater. Interfaces 10 (2018) 27669–27680. [PubMed: 30063134]
62. Mohiuddin OA, Campbell B, Poche JN, Ma M, Rogers E, Gaupp D, Harrison MAA, Bunnell BA, Hayes DJ, Gimble JM. Decellularized Adipose Tissue Hydrogel Promotes Bone Regeneration in Critical-Sized Mouse Femoral Defect Model. Front Bioeng Biotechnol. 7 (2019) 211. [PubMed: 31552237]
63. Li M, Zhang C, Mao Y, Zhong Y, Zhao J, A Cell-Engineered Small Intestinal Submucosa-Based Bone Mimetic Construct for Bone Regeneration.Tissue Eng Part A 24 (2018) 1099–1111. [PubMed: 29318958]
64. Meury T, Verrier S, Alini M, Human endothelial cells inhibit BMSC differentiation into mature osteoblasts in vitro by interfering with osterix expression. J Cell Biochem. 98 (2006) 992–1006. [PubMed: 16479590]
65. Yousif LF, Di Russo J, Sorokin L. Laminin isoforms in endothelial and perivascular basement membranes. Cell Adh Migr 7 (2013) 101–110. [PubMed: 23263631]
66. Bouletreau PJ, Warren SM, Spector JA, Peled ZM, Gerrets RP, Greenwald JA, Longaker MT MT, Hypoxia and VEGF up-regulate BMP-2 mRNA and protein expression in microvascular endothelial cells: implications for fracture healing.Plast Reconstr Surg (109) 2002 2384–2397. [PubMed: 12045566]
67. Fiedler J, Brill C, Blum WF, Brenner RE, IGF-I and IGF-II stimulate directed cell migration of bone-marrow-derived human mesenchymal progenitor cells. Biochem Biophys Res Commun 345 (2006)1177–1183. [PubMed: 16716263]
68. Kanaan RA, Aldwaik M, Al-Hanbali OA, The role of connective tissue growth factor in skeletal growth and development. Med Sci Monit 12 (2006) 277–281.
69. Grellier M, Bordenave L, Amédée J, Cell-to-cell communication between osteogenic and endothelial lineages: implications for tissue engineering. Trends Biotechnol (27) 562–571. [PubMed: 19683818]
70. Qi P, Zhou Y, Wang D, He Z, Li Z, A new collagen solution with high concentration andcollagen native structure perfectly preserved. RSC Adv. 5 (2015) 87180–87186.
71. Gast K, Siemer A, Zirwer D, Damaschun G, Fluoroalcohol-induced structural changes ofproteins: Some aspects ofcosolvent-protein interactions. Eur. Biophys. J 30 (2001) 273–283. [PubMed: 11548130]
72. Sisson K, Zhang C, Farach-Carson MC, Chase DB, Rabolt JF JF, Fiber diameters control osteoblastic cell migration and differentiation in electrospun gelatin. J Biomed Mater Res A. 94 (2010) 1312–1320. [PubMed: 20694999]
73. Eichhorn SJ, Sampson WW, Statistical geometry of pores and statistics of porous nanofibrous assemblies. J. Roy. Soc. Interface 2 (2005) 309–318. [PubMed: 16849188]
74. Bai L, Li Q, Duo X, Hao X, Zhang W, Shi C, Guo J, Ren X, Feng Y, Electrospun PCL-PIBMD/SF blend scaffolds with plasmid complexes for endothelial cell proliferation. RSC Adv. 7 (2017) 39452–39464.
75. Badami AS, Kreke MR, Thompson MS, Riffle JS, Goldstein AS, Effect of fiber diameter on spreading, proliferation, and differentiation of osteoblastic cells on electrospun poly(lactic acid) substrates. Biomaterials 27 (2006) 596–606. [PubMed: 16023716]
76. Liao J, Guo X, Nelson D, Kasper FK, Mikos AG, Modulation of osteogenic properties of biodegradable polymer/extracellular matrix scaffolds generated with a flow perfusion bioreactor. Acta Biomater. 6 (2010) 2386–2393. [PubMed: 20080214]
77. Decaris ML, Mojadedi A, Bhat A, Leach JK, Transferable cell-secreted extracellular matrices enhance osteogenic differentiation. Acta Biomater. 8(2012) 744–752. [PubMed: 22079209]

78. Zhao G, Bao X, Huang G, Xu F, Zhang X, Differential Effects of Directional Cyclic Stretching on the Functionalities of Engineered Cardiac Tissues. ACS Applied Bio Materials 2 (2019) 3508–3519.

Highlights

- Decellularized extracellular matrices (dECMs) retain their bioactivity after embedding into a synthetic polymer.
- dECM source predicts osteoblast mineralization *in vitro* in tissue specific manner.
- In implanted scaffold with two distinct extracellular matrices, both matrices synergistically contribute to cortical bone regeneration.
- The nanofibrous architecture of the scaffold blocks tissue infiltration and might serve as a cell migration bridge in bone defects *in vivo*.

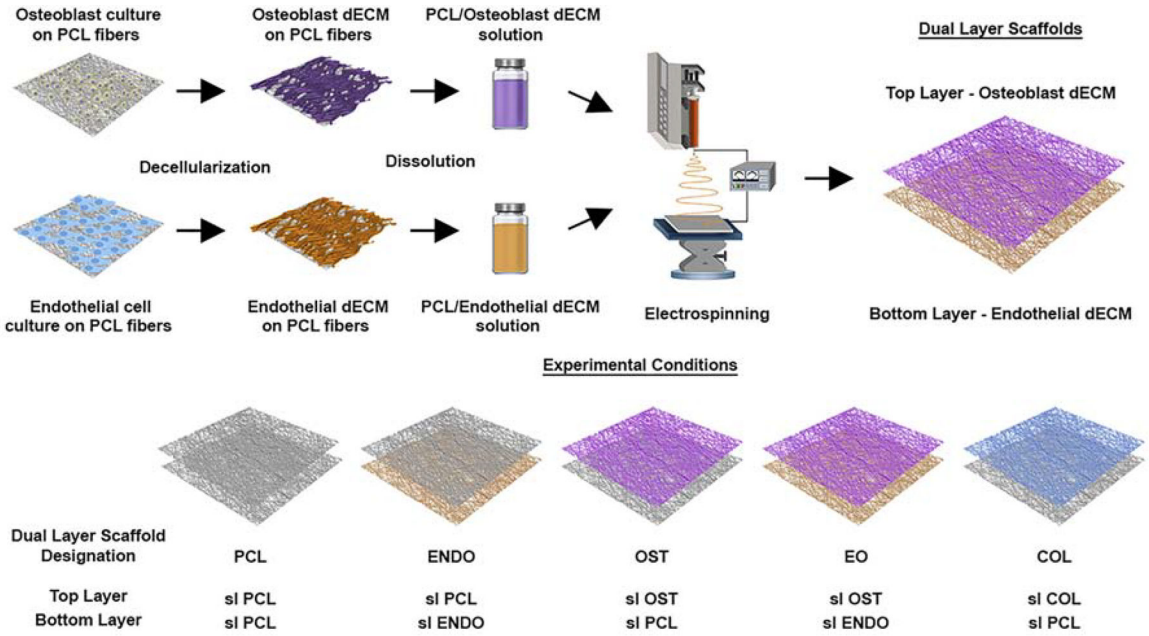

Fig. 1.

A schematic representation of the electrospinning fabrication process of nanofibrous dual-layer scaffolds with embedded decellularized ECM from osteoblasts and endothelial cell cultures in fibers.

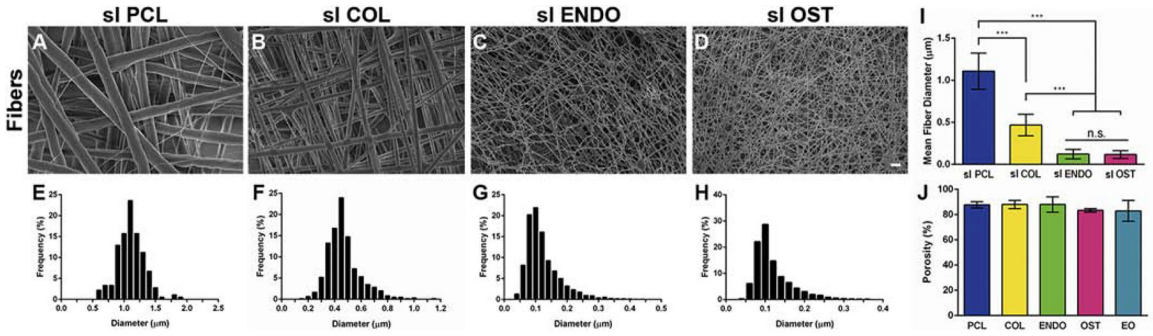

Fig. 2.

Scanning electron microscopy images depicting morphology of electrospun (A) PCL, (B) PCL-collagen (COL), (C) PCL-endothelial dECM (ENDO), (D) PCL-osteoblast dECM (OST) fibers. Histogram of fiber diameter distribution for (E) PCL, (F) COL, (G) ENDO, (H) OST fiber groups. Average fiber diameter (I) of PCL fibers and fibers with embedded dECM protein. Percentage of porosity (J) measured for each group in dual-layer scaffolds. *** $P<0.0001$. n.s. $P>0.05$. Scale bar 10μm.

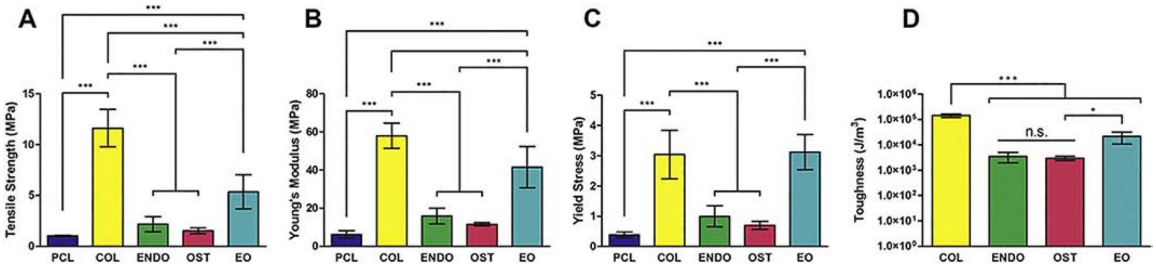

Fig. 3.

Mechanical properties of dual-layer PCL-dECM scaffolds after tensile testing. Ultimate tensile strength (A), Young's modulus (B), yield stress (C), and toughness (work to fracture) (D). **P*<0.01. ****P*<0.0001. n.s. P>0.05.

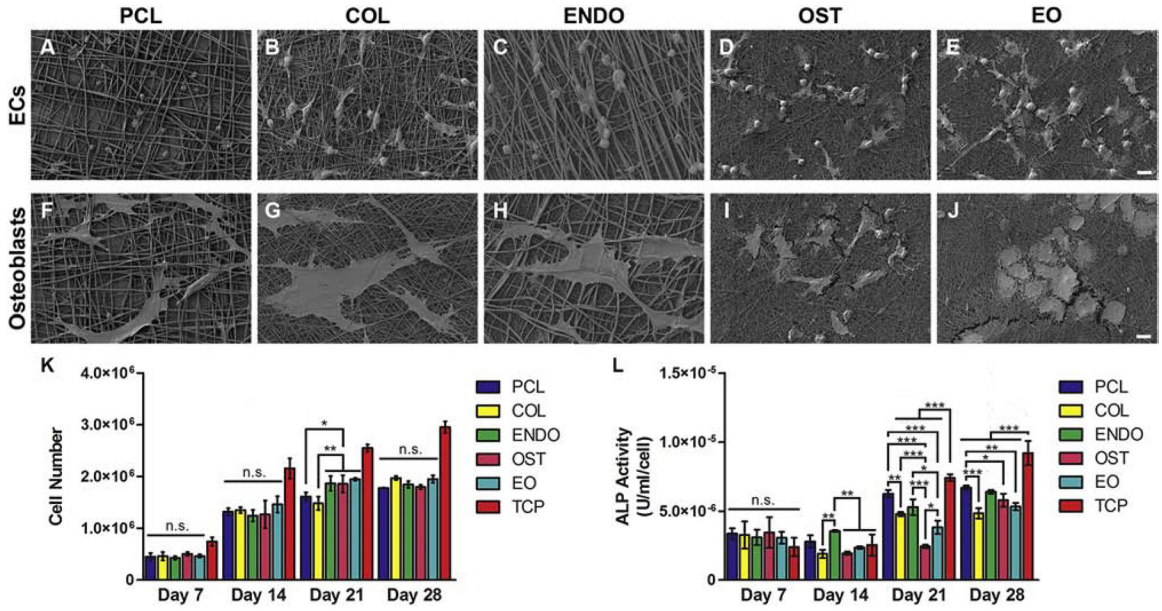

Fig. 4.

Cell attachment and growth response *in vitro* to PCL-dECM fibers. Cell morphology depicted using scanning electron microscopy of endothelial cells (A-E) and osteoblasts(F-J) attached to dual layer PCL (A,F), COL (B,G), ENDO (C,H), OST (D,I), and EO (E,J)scaffolds. Cell number of osteoblasts (K) cultured for 7, 14, 21, and 28 days on dual layer PCL scaffolds (PCL) with dECM from endothelial cells (ENDO), osteoblasts (OST), and osteoblast and endothelial cell dECM in separate layers (EO). Enzymatic activity measurement of Alkaline Phosphatase (ALP) secreted by osteoblasts cultured on PCL scaffolds with embedded dECM(L) at day 7, 14, 21, and 28. Values are expressed as mean ± SD. **P*<0.01. ***P*<0.001. ****P*<0.0001. n.s. P>0.05. Scale bar 10 μm.

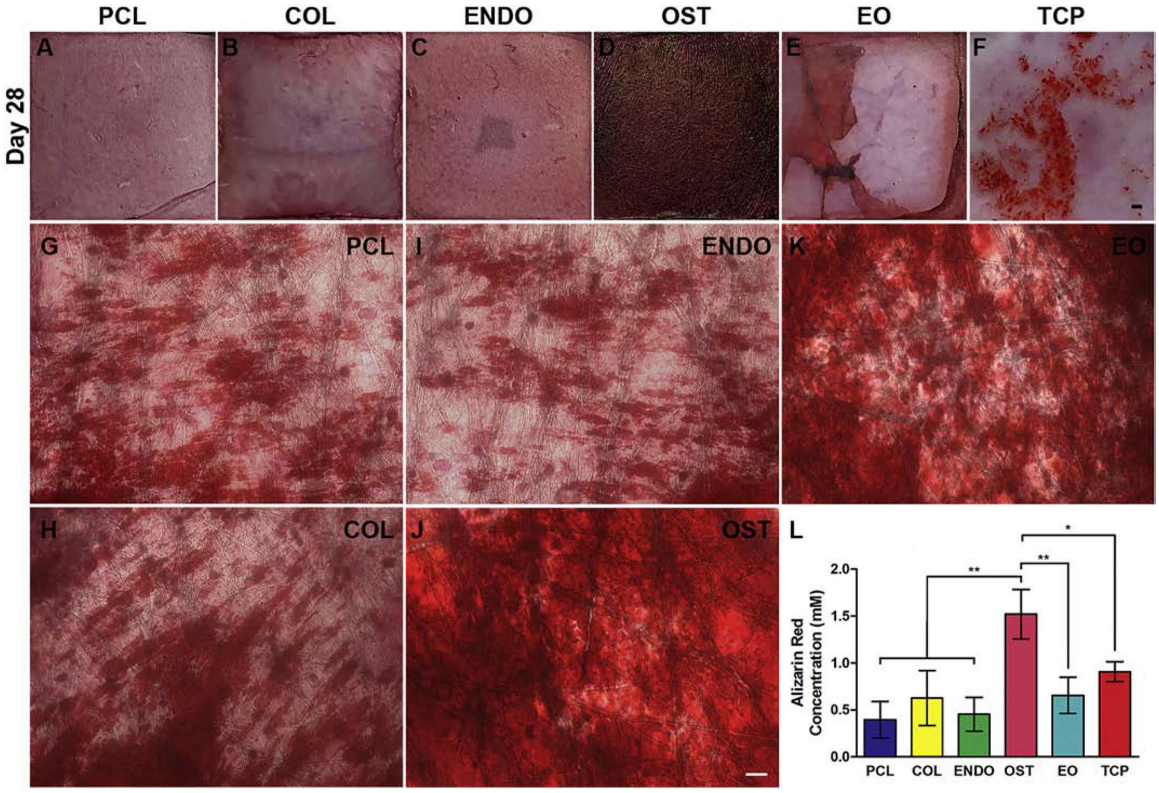

Fig. 5.

Alizarin Red S (ARS) staining of osteoblast calcium mineral deposits (red) after 28 days of culture (A-K). Cells were cultured tissue culture plate (TCP, F) and on PCL fibrous scaffolds mounted on a coverglass (A,G) as controls. Nanofibrous scaffolds with embedded collagen (COL) (B,H), endothelial dECMs (ENDO)(C,I), osteoblasts dECM (OST) (D,J), or endothelial/osteoblasts dECM in separate fiber layers (EO) (E,K). Images at lower magnification show entire scaffold and the extent of mineralization (A-F).Higher magnification show relative areas and intensity of mineral deposit staining on the scaffold (G-K). For stereomicroscope images (A-F), scale bar 5 mm. For optical microscope images (G-K), scale bar 100 μm. Concentration of ARS abound to calcium mineral deposits extracted from Day 28 cultures with cetylpyridinium chloride (U). Values are expressed as mean ± SD. *P<0.01. **P<0.001.

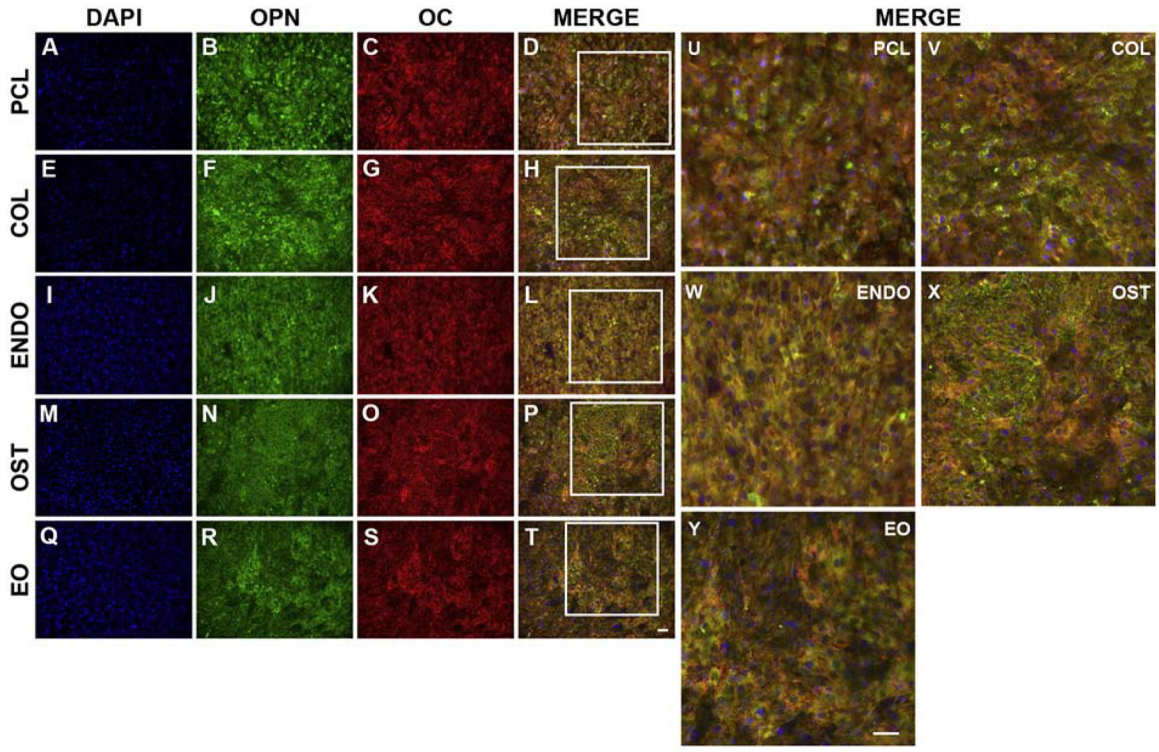

Fig. 6.

Immunostaining of osteocalcin (OC) and osteopontin (OPN) extracellular deposits secreted by osteoblasts cultured on PCL fibers with embedded collagen (COL) (E,F,G,H,V), endothelial dECM (ENDO) (I,J,K,L,W), osteoblast dECM (OST) (M,N,O,P,X), and endothelial/osteoblast dECM in separate layers (EO) (Q,R,S,T,Y). Osteoblasts cultured on PCL scaffolds were stained as controls (A, B, C, D, U). Cells were stained with a nuclear stain DAPI (A,E,I,M,Q) (blue), antibodies against OPN (B,F,J,N,R) (green), and antibodies against OC (C, G, K, O,S) (red).To identify extracellular and intracellular OPN and OC, images were merged (MERGE) (D,H,L,P,T,U,V,W,X,Y). Boxes in D,H,L,P,T indicate regions imaged in U,V,W,X,Y, respectively. Scale bar 200 μm.

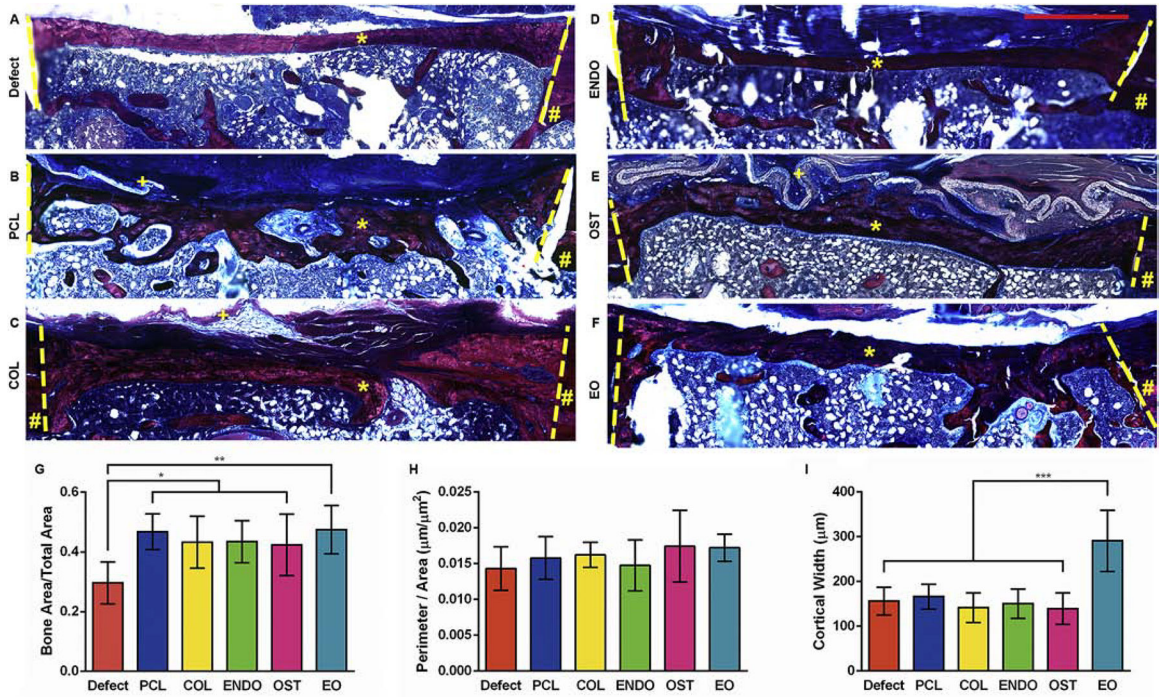

Fig. 7.

Representative histological examination of decalcified femurs 6 weeks postsurgery with different treatments: untreated control (A, Defect), dual-layer PCL scaffold (B, PCL), scaffold with embedded collagen (C, COL), scaffold with embedded endothelial dECM (D, ENDO), scaffold with embedded osteoblast dECM (E, OST), and scaffold with endothelial/osteoblast dECM (F, EO).Sections were stained with Masson's Trichrome stain. Lines indicate boundaries of defects. # indicates uninjured cortical bone. * indicates regenerate bone. + indicates un-degraded scaffold. Histomorphological analysis of femur sections showing new bone formation per unit area (G), total perimeter of new bone formation per unit area (H), and cortical width (I). For each measurement, the images of 8 sections were used. Values are expressed as mean ± SD. *P<0.01. **P<0.001. ***P<0.0001. Scale bar 1mm.

Table 1.

Electrospinning parameters

	Parameters
Solvent	HFIP/FA/DMSO (8:1:1)
Voltage	10–12 kV
Flow rate	0.25 mL/h
Distance	10 cm
Spinning time per layer	10 minutes
Needle Gauge (GA)	20 G